RSC Advances

ROYAL SOCIETY OF CHEMISTRY

www.rsc.org/advances

Journal Name

ARTICLE

Remarkable enhancement of photovoltaic performance of ZnO/CdTe core-shell nanorod array solar cells through interface passivation with TiO_2 layer

Received 00th January 20xx,
Accepted 00th January 20xx

DOI: 10.1039/x0xx00000x

www.rsc.org/

Guanghui Zhang[a], Yukun Wu[a], Huaiyi Ding[b], Yunsong Zhu[a], Junwen Li[a], Yue Lin[b], Shenlong Jiang[b,c], Qun Zhang[b,c], Nan Pan[b,c], Yi Luo[b,c] and Xiaoping Wang[a,b,c]*

All-inorganic solid-state ZnO/CdTe core-shell nanorod array solar cells (NRASCs) have been fabricated by a simple low-temperature and low-cost chemical solution method. A thin TiO_2 layer with different thickness was introduced at the ZnO/CdTe interface using atomic layer deposition and its effect on the photovoltaic performance of the NRASCs was investigated. It is found that the overall power conversion efficiency of the ZnO/TiO_2 (4 nm)/CdTe NRASC can reach up to 1.44% under AM 1.5G illumination (100 mW/cm^2), which is about 6 times of the NRASC without TiO_2 layer. By further systematic characterizations, we find that the thin TiO_2 layer, serving as an efficient passivation and blocking layer at the interface of ZnO/CdTe nanorod, can remarkably suppress the charge recombination at the interface but negligibly affect the light absorption and the charge separation efficiency, thus leading to significant increases of the carrier lifetime and the open-circuit voltage of the NRASCs. This result expands the knowledge and opportunities for low-cost, high-performance NRASCs through simple interface engineering.

Introduction

Various nanomaterials and nanostructures have been developed recently to make low-cost, high-performance solar cells.[1-4] Well-aligned one-dimensional nanostructure has attracted exceptionally significant attention for its excellent light trapping and antireflection properties, rendering the enhancement of light absorption for solar cells.[5, 6] In particular, core-shell nanorod array solar cell (NRASC), in which the nanorod core is covered by other type of semiconductor shell to form a p-n junction in the radial direction, allows light absorption in the axial direction and charge separation in the radial one. By virtue of this unique architecture, it enables strong light absorption as well as efficient charge separation and transport, promising an overall improvement of power conversion efficiency. More importantly, the NRASC can even be composed of materials with short minority carrier diffusion length, providing an alternative access to produce high-efficiency photovoltaic devices *via* low-cost materials.

Among NRASC materials, n-type ZnO nanorod arrays (NRAs) are widely used as the electron transport component because of the high electron mobility and facile synthesis.[7-11] Meanwhile, p-type CdTe is a promising active material for photovoltaics because of its nearly ideal band gap for single-junction solar cells and large optical absorption coefficient. In addition, a type-II energy band alignment is well defined between CdTe and ZnO, which can facilitate the separation of the electron-hole pairs.[9, 12, 13] However, despite the aforementioned advantages, only a few ZnO/CdTe NRASCs have been reported and the corresponding performances are not as high as expected yet.[12, 14-16] Besides, the solar cells based on core-shell nanostructures always suffer from the low open-circuit voltage (V_{oc}) and fill factor (FF) due to the severe charge recombination process occurred through the interface. Therefore, avoiding the charge carrier from the recombination is vital for improving the power conversion efficiency of core-shell NRASCs. To this end, various materials, such as TiO_2,[17-19] Al_2O_3[20] and ZrO_2[21] have been introduced at the interface to increase the lifetime of minority carrier and enhance the device performance. Among these materials, TiO_2 is most commonly used as an electron acceptor in photovoltaic devices owing to its good chemical stability.[1] Moreover, since TiO_2 has the similar valence band (VB) and conduction band (CB) energy levels as those of ZnO, it can efficiently passivate the surface defect of ZnO NR without degradation of the carrier transport. For example, Tian *et al.* introduced TiO_2 nanosheets on the surface of ZnO NR in quantum dot sensitized solar cells to prolong the electron lifetime and increase the V_{oc}.[18]

In this work, we fabricated solid-state ZnO/CdTe core-shell NRASCs through depositing the CdTe shell onto the hydrothermally-grown ZnO NRs using a low-cost successive ionic layer adsorption and reaction (SILAR) method.[22-24] A thin TiO_2 layer, with various thicknesses of 0.5, 1, 2, and 4 nm respectively, was introduced at the core/shell interface by

[a] Department of Physics, University of Science and Technology of China, Hefei 230026, P. R. China.
[b] Hefei National Laboratory for Physical Sciences at the Microscale, University of Science and Technology of China, Hefei 230026, P. R. China.
[c] Synergetic Innovation Center of Quantum Information & Quantum Physics, University of Science and Technology of China, Hefei, Anhui 230026, P. R. China. E-mail: xpwang@ustc.edu.cn; Tel: +86-551-3607090.

† Electronic Supplementary Information (ESI) available: See DOI: 10.1039/x0xx00000x

atomic layer deposition (ALD) to reduce the interfacial charge recombination. The architecture of our solar cell is schematically shown in Fig. 1a. The photovoltaic performances of these ZnO/CdTe and ZnO/TiO_2/CdTe NRASCs have been systematically investigated. We found that the V_{oc} of the solar cell is only 165 mV for ZnO/CdTe NRASC, but can increase dramatically after inserting the TiO_2 layer and reach to 627 mV for ZnO/TiO_2 (4 nm)/CdTe NRASC. At the same time, the short-circuit current density (J_{sc}) and FF is also slightly improved by the thin TiO_2 interfacial layer. Consequently, the overall power conversion efficiency of the ZnO/TiO_2 (4 nm)/CdTe NRASC can reach up to 1.44%, which is about 6 times of ZnO/CdTe NRASC.

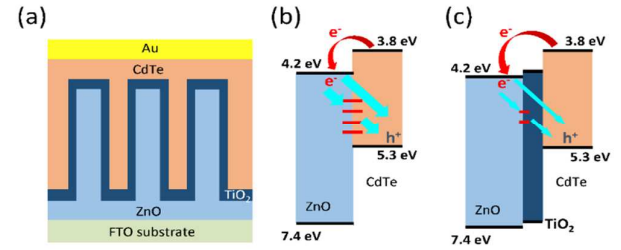

Fig. 1 (a) Schematic of the ZnO/TiO_2/CdTe core-shell NRASC. (b and c) The energy level as well as the carrier transport and recombination path of ZnO/CdTe (b) and ZnO/TiO_2/CdTe core-shell NRASC (c).

Experimental section

Synthesis of ZnO NRAs

ZnO NRAs were synthesized using a two-step procedure of seeding and hydrothermal growth on patterned fluorine-doped tin oxide (FTO) coated glass substrates.[25, 26] The sheet resistance of the FTO is 15 Ω/cm^2. The 2×2 cm^2 FTO slides were cleaned and dried before a ZnO nanocrystal seed layer was prepared by spin coating the sol-gel precursor containing 0.75 M zinc acetate dihydrate in 2-methoxyethanol with a 1:1 ratio at 1200 rpm and subsequent annealing in air at 400 °C for 10 minutes. ZnO NRAs were then hydrothermally grown from the seed layer in a solution containing 30 mM zinc nitrate and equivalent hexamethylenetetramine at 92 °C for 90 minutes.

ALD of TiO_2

TiO_2 was deposited onto the ZnO NRAs using an ALD system (MNT-100, Wuxi MNT Micro and Nanotech). Tetrakis(dimethylamino)titanium and water were used as the titanium and oxygen precursors, respectively. The deposition was performed at 120 °C under a base pressure of 42 Pa. Each cycle of ALD consists of 40 ms Ti precursor pulse with 25 s N_2 purging and 6 ms water pulse with 30 s N_2 purging. The thickness of TiO_2 layer was controlled by the ALD cycles.

CdTe shell deposition

The CdTe shell was deposited using SILAR method.[22-24] $Cd(NO_3)_2{\cdot}4H_2O$ was used as the Cd^{2+} sources. Te^{2-} was prepared from Te powder reduced by $NaBH_4$ with N_2 protection. Then the CdTe was deposited under N_2 atmosphere to prevent the oxidation of Te^{2-}, the concentration for both precursor solutions was 0.1 M. Typically, in each cycle of CdTe SILAR process, the substrate was immersed into Cd^{2+} solution for 15 s and rinsed by deionized water; followed by 15 s immersion in Te^{2-} solution and rinsing. After 60 cycles, CdTe was fully filled the interspace of the NRAs. After deposition, the samples were pre-annealed at 150 °C for 2 min, immediately followed by immersion into a 60 °C solution of saturated $CdCl_2$ in methanol, rinsing with 1-PrOH and subsequent annealing in air at 400 °C for 10 minutes.[27]

Device fabrication and characterization

ZnO/CdTe and ZnO/TiO_2 (0.5, 1, 2, 4 nm)/CdTe core-shell NRASCs were fabricated by thermally evaporating 100 nm Au on the top of these NRAs through a shadow mask to form 2×2 mm^2 top electrodes. The morphologies were observed by a FEI Sirion 200 scanning electron microscope (SEM). The microstructure and energy dispersive X-ray spectrum (EDS) of single NRs were performed on a JEOL-2010 transmission electron microscope (HRTEM/TEM) operated at 200 kV. The crystal structure was analyzed by a PHILIPS X'PERT PRO X-ray diffractometer (XRD) with Cu *Kα* line (*λ*=1.54184 Å). UV-Vis absorption spectra were obtained on U-4100 spectrophotometer (HITACHI). Photoluminescence (PL) was collected on Fluorolog3-TAU. Ultrafast transient absorption (TA) spectroscopy was performed with a 25 fs Ti:sapphire laser system.

For solar cell performance testing, all current density-voltage (J-V) curves were measured under ambient condition using a Keithley 2400 sourcemeter. The AM 1.5G simulated sunlight illumination of 100 mW/cm^2 was obtained by a 94023A Oriel Sol3A solar simulator (Newport) and calibrated with a reference silicon solar cell. The electrochemical impedance spectroscopy was carried out in the dark at room temperature using a CHI 660E electrochemical workstation (Shanghai Chenhua Instruments Co.). Open-circuit voltage decay (OCVD) measurement was performed using a chopped 532 nm laser while monitoring the subsequent decay of the open-circuit voltage by an oscilloscope (Tektronix TDS 2012).

Results and discussion

A series of ZnO NRAs with different thickness TiO_2 coating have been fabricated by ALD deposition. The CdTe shell active layer was subsequently deposited onto the ZnO/TiO_2 NRs using SILAR method. It is found that CdTe can fully fill the interspace of the ZnO/TiO_2 array after 60 cycle deposition. To improve the interfacial contact of the core-shell structures and the crystallinity of shell layers, the samples were further treated by $CdCl_2$ and annealed in air at 400 °C for 10 minutes.[27]

Fig. 2a reveals the X-ray diffraction (XRD) patterns taken from the bare ZnO, ZnO/TiO_2 (2 nm) NRAs as well as the annealed ZnO/CdTe and ZnO/TiO_2 (2 nm)/CdTe core-shell NRAs, respectively. For the bare ZnO NRs, besides the peaks of FTO, only ZnO (002) peak can be found, suggesting that the

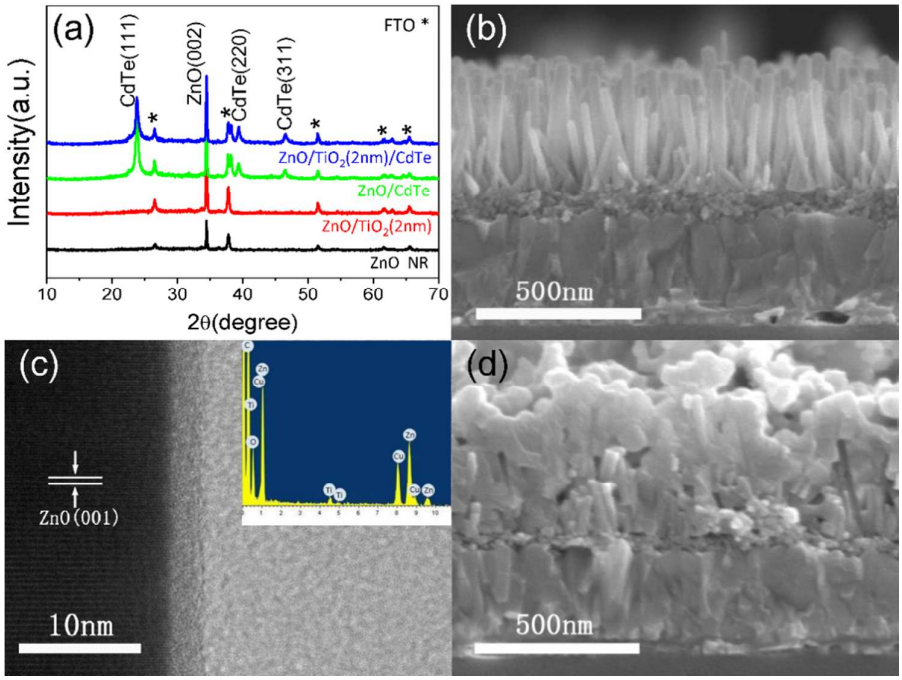

Fig. 2 (a) XRD patterns of the bare ZnO, ZnO/TiO_2 (2 nm), annealed ZnO/CdTe and ZnO/TiO_2 (2 nm)/CdTe NRAs. (b) The typical cross-sectional SEM image of ZnO/TiO_2 (2 nm) NRAs. (c) HRTEM image and EDS (inset) of a single ZnO/TiO_2 (2 nm) NR. (d) The typical cross-sectional SEM image of annealed ZnO/TiO_2 (2 nm)/CdTe core-shell NRAs.

ZnO NRs grew dominantly along the c-axis orientation. The result for the ZnO/TiO_2 (2 nm) sample is very similar to that of the bare ZnO. After the CdTe layer was deposited and annealed, three new diffraction peaks are observed at 23.74, 39.40 and 46.42°, which can be indexed to the (111), (220) and (311) planes of zinc-blende CdTe (JCPDS file No.65-1085), respectively. No signal from the oxide phase, such as CdO or TeO_2, can be detected. Moreover, the average grain size of CdTe for both ZnO/CdTe and ZnO/TiO_2/CdTe samples are the same as about 20 nm, indicating the thin TiO_2 layer has negligible effect on the crystallinity of the CdTe shells.

Fig. 2b shows the cross-sectional SEM image of a ZnO/TiO_2 (2 nm) NRA on FTO substrate. The NRs show uniform morphology and the length is ~ 360 nm. The microstructure and composition of the NRs were further investigated by TEM and EDS. Fig. 2c shows a typical HRTEM image of a single ZnO/TiO_2 (2 nm) NR, the ZnO NR shows perfect single-crystal wurtzite structure with clear stacking along its c-axis, consistent with the XRD result in Fig. 2a. In addition, a uniform amorphous TiO_2 thin layer can be found covering on the surface of the ZnO NR, whose thickness is estimated to be about 2 nm. The Ti element can be confirmed from the EDS result shown in the inset of Fig. 2c. Fig. 2d demonstrates the cross-sectional SEM image of an annealed ZnO/TiO_2 (2nm)/CdTe core-shell NRA, from which the very compacted film-like filling with few voids can be observed.

ZnO/TiO_2/CdTe core/shell NRASCs with different TiO_2 (0, 0.5, 1, 2 and 4 nm) thicknesses have been fabricated to investigate the effect of TiO_2 layer on the photovoltaic performances. Fig. 3a, b show the typical steady-state J-V curves of the solar cells in the dark and under AM 1.5G illumination of 100 mW/cm^2, respectively. As seen in Fig. 3a, all curves show the good rectifying behaviour and the positive dark current decreases with the increasing thickness of TiO_2 layer. Fig. 3b demonstrates that the thin TiO_2 layer can significantly improve the photovoltaic performance of the NRASCs. The thickness dependence of the NRASC performances, such as J_{sc}, V_{oc}, FF and power conversion efficiency η, are further summarized in Fig. 3c,d. (The detailed device characteristics are listed in Table S1). Obviously, V_{oc} increases by near 4-fold from 165 mV for ZnO/CdTe NRASC to 602 mV for ZnO/TiO_2 (2 nm)/CdTe NRASC and saturates for ZnO/TiO_2 (4 nm)/CdTe NRASC. At the same time, both J_{sc} and FF of the NRASCs increase slightly with the TiO_2 layer thickness. Consequently, the overall power conversion efficiency of the ZnO/TiO_2 (4 nm)/CdTe NRASC dramatically enhances and reaches up to 1.44%, about 6 times of the NRASC without TiO_2.

We now turn to study the underlying reason in the following sections why the ZnO/TiO_2/CdTe core-shell NRASC possesses much higher photovoltaic performance as compared to the ZnO/CdTe one. In principle, the photon to current conversion efficiency of a solar cell is dominantly determined by three processes including the photon absorption, the charge separation, and the carrier transport and collection. To investigate whether the interfacial thin TiO_2 layer can alter the absorption of the solar cells, UV-Vis absorbance spectra were

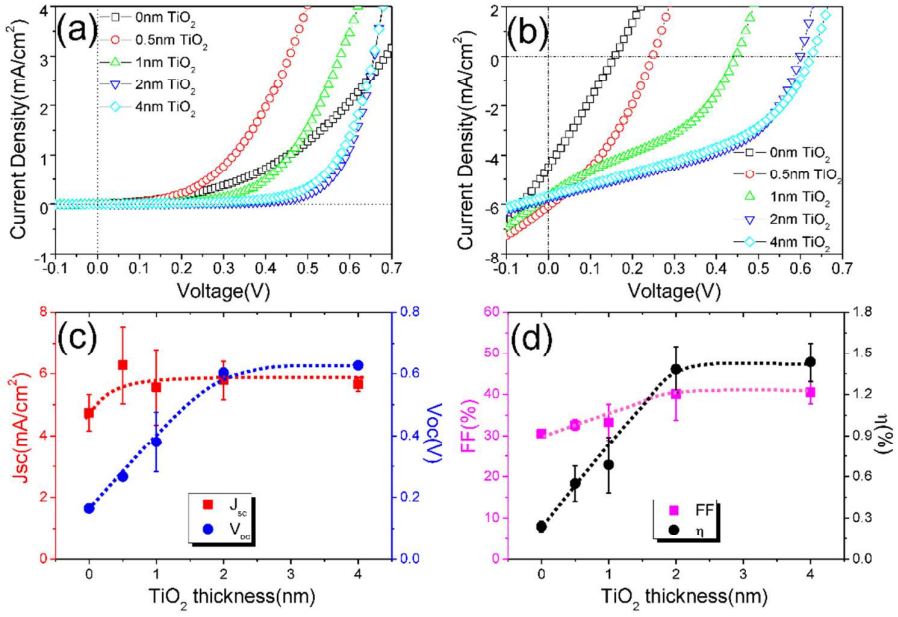

Fig. 3 J-V curves of ZnO/TiO_2/CdTe core-shell NRASCs with 0, 0.5, 1, 2, and 4 nm thick TiO_2 layers (a) in the dark and (b) under AM 1.5G illumination of 100mW/cm^2. (c) J_{sc} and V_{oc}, (d) FF and η versus the thickness of TiO_2 layer. Error bars are obtained from six devices for each kind of NRASC, and the dotted lines are guide for eyes.

measured on the bare ZnO, ZnO/TiO_2 (0.5, 1, 2, 4 nm), annealed ZnO/CdTe and ZnO/TiO_2 (0.5, 1, 2, 4 nm)/CdTe NRAs and the results are shown in Fig. S1. It is found that the ZnO and ZnO/TiO_2 NRAs have the same absorption edge at ~ 380 nm and the absorption intensity increases slightly with the thickness of TiO_2 layer. However, for the ZnO/CdTe and ZnO/TiO_2/CdTe core-shell NRAs, the absorption edge shifts obviously to 850 nm, consistent with the band gap of bulk CdTe.[28, 29] It is notable that the ZnO/TiO_2/CdTe NRs with different TiO_2 thicknesses have almost the same absorption behaviour, indicating that the CdTe shell is the dominant light-absorption material in the above mentioned core-shell nanostructures. Therefore, we can conclude that the enhanced photovoltaic performance of the NRASC after inserting TiO_2 layer cannot be ascribed to the change of light absorption.

It is well known that a type II energy band alignment is beneficial for separating the photocarriers. For the case of ZnO/CdTe NRAs as shown in Fig. 1, this results in the photoinduced electrons of CdTe shell injecting into the ZnO core. In order to investigate whether the TiO_2 interfacial layer will prompt the charge separation in the core-shell NRASCs, we measured the transient absorption spectra on the ZnO/TiO_2/CdTe NRAs with different TiO_2 thicknesses, since the method has been extensively practiced in photovoltaic devices.[30-32] The measurements were performed on a 25 fs Ti:sapphire laser system. Each sample was excited by a 400 nm pump light and the excited state absorption signals were probed at 630 nm, the results are shown in Fig. S2. As seen, the decay of the excited state absorption are almost the same and do not show any dependence on the thickness of TiO_2, suggesting that the TiO_2 layer has negligible contribution to the charge separation at the ZnO/CdTe interface.

It has been reported that the charge recombination has a notable impact on the V_{oc} and the power conversion efficiency of solar cells.[11, 33, 34] This can be understood by the band alignment as well as the electron transport and recombination path in the core-shell NRASC shown in Fig. 1b, c. Under light illumination, the photoinduced electron-hole pairs in the CdTe shell are separated rapidly at the interface; The electrons are injected into the ZnO and then transported to the FTO electrode, while the holes remain in the CdTe shell are collected by the Au electrode. However, the electrons would meanwhile recombine with the holes at the interface. At the open-circuit condition, the photocurrent exactly balances the forward bias current which is dependent on the recombination process. Therefore, low recombination decreases the forward bias current for p-n junction, which in turn shifts the balance at a higher V_{oc}. In the case of ZnO/CdTe, as shown in Fig. 1b, the electrons in ZnO are easily trapped by the ZnO surface defects and recombine with the holes in CdTe, leading to the increase of the shunt current and decrease of the V_{oc}. In sharp contrast, for ZnO/TiO_2/CdTe NRASCs as shown in Fig. 1c, a natural speculation is that the TiO_2 layer could passivate the ZnO surface defects and act as a blocking layer to suppress the electron-hole recombination at the interface, thus increasing the shunt resistance and the V_{oc}. The decrease of charge recombination at the interface after coating TiO_2 can even been observed from the dark J-V curves, as shown in Fig. 3a,

the dark-recombination current decreases as the TiO_2 layer thickness increases at positive bias.

To further verify the passivation effect of the TiO_2 layer on reducing the ZnO surface defects and improving the performance of the ZnO/TiO_2/CdTe NRASC, three distinct experimental measurements, including photoluminescence (PL), impedance spectroscopy and open-circuit voltage decay behaviour are carried out sequentially. Room temperature PL was collected on bare ZnO NRA and ZnO/TiO_2 (0.5, 1, 2 nm) NRAs, the results are shown in Fig. S3. We can find that all of the PL spectra have the both emission bands of ZnO: a narrow peak from near band edge (NBE) emission at 375 nm and another broad band from deep level emission (DLE) around 565 nm. The origin of DLE is usually attributed to the surface defects of ZnO NR.[35, 36] As seen, after coating TiO_2 layer on ZnO NR, the intensity of NBE increases whereas that of DLE decreases; Specifically, the trend that the I_{DLE}/I_{NBE} ratio decreases with the increasing thickness of TiO_2 from 0 to 1 nm and gets saturated at 2 nm can be clearly observed in the inset of Fig. S3. This finding suggests that the thin TiO_2 layer can effectively passivate the surface defects of the ZnO NRs. As a result, the photovoltaic performance of the ZnO/TiO_2/CdTe NRASC can be improved by virtue of the reduced charge recombination through the defects.

The impedance spectroscopy, which has been widely used to analyze the charge recombination process and electron lifetime in solar cells,[37, 38] was also measured here with a two-electrode configuration[9] (the FTO as the working electrode and the Au electrode as both the counter- and the reference electrodes). We performed the experiment in the dark by applying a sinusoidal perturbation of 10 mV with the frequency changing from 100 kHz to 0.1 Hz. Fig. 4a shows the results of the ZnO/TiO_2/CdTe NRASCs with the TiO_2 thickness varying from 0 to 4 nm. The equivalent circuit of the solar cells is shown in the inset, where R_s is the series resistance, R_{sh} is the shunt resistance (interfacial charge recombination resistance) and C is the capacitance, respectively. Note that R_s is totally contributed from the ZnO nanorod, TiO_2 passivation layer, CdTe shell, as well as their contact resistance with the electrodes, and consequently, it is dependent on the thickness of TiO_2 layer. The electron lifetime t_n can be determined from the time constant of the impedance spectrum according to:[39, 40]

$$t_n = \frac{1}{2\pi f_c} \quad (1)$$

where f_c is the characteristic frequency of the impedance spectrum. In this way, all parameters of R_s, R_{sh}, C and t_n corresponding to the NRASCs can be obtained by fitting the experimental results of the impedance spectra (The detailed results are listed in Table S2). Fig. 4b shows the R_{sh} and t_n as a function of the TiO_2 thickness. It is found that, as the thickness of the TiO_2 layer varies from 0 to 2 nm, the R_{sh} increases from 54 kΩ for ZnO/CdTe NRASC to 390 kΩ for ZnO/TiO_2 (2 nm)/CdTe one while the corresponding t_n also increases by two orders of magnitude (from 0.43 to 62.4 ms). The result strongly indicates that the charge recombination is effectively suppressed and the electron lifetime is drastically prolonged through the simple interface passivation by the thin TiO_2 layer. Also worth noting is that the charge recombination probably also occurs in the amorphous TiO_2 layer (see TEM characterization in supplementary information of Fig.S4), which makes the R_{sh} of the NRASC with 4 nm TiO_2 becomes smaller than the maximum. Therefore, one can obtain an optimal passivation thickness between 2~4 nm for the ZnO/TiO_2/CdTe NRASCs.

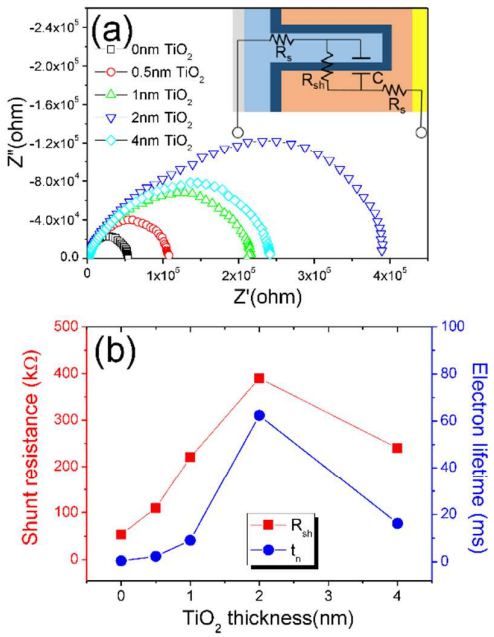

Fig. 4 (a) Impedance spectra of the ZnO/TiO_2/CdTe NRASCs with the TiO_2 thickness varying from 0 to 4 nm. The inset shows the equivalent circuit for the solar cells. R_s, series resistance; R_{sh}, shunt resistance; C, capacitance. (b) Shunt resistance R_{sh} and electron lifetime t_n as a function of the TiO_2 layer thickness.

The open-circuit voltage decay method was also applied to further investigate the charge recombination and electron lifetime of the solar cells.[19, 41, 42] In each measure, the NRASC was first illuminated by a 532 nm laser to a steady V_{oc}, then the incident light was turned off periodically using a chopper, and the subsequent decay of the V_{oc} was monitored by an oscilloscope. When the light is turned off, the electrons in the ZnO NR will recombine with the holes in the CdTe shell. This shifts the electron quasi-Fermi level of the ZnO downwards and the hole quasi-Fermi level of the CdTe upwards, thus leading to the V_{oc} getting smaller and smaller until the quasi-Fermi level of electron equilibrates in ZnO with that of hole in CdTe, *i.e.*, the V_{oc} becomes zero. Fig. 5a demonstrates the V_{oc}-time decay traces of the ZnO/TiO_2/CdTe NRASCs with different TiO_2 thicknesses. As seen, the V_{oc} of all devices decrease rapidly after turning off the light. It is important to find that the thicker the TiO_2 layer, the longer the V_{oc} decay time, demonstrating the unambiguous blocking effect of TiO_2 on the carrier recombination. Quantitatively, the electron lifetime can be derived from the decay curve with following equation:[41, 43]

$$\tau_n = -\frac{kT}{q}\left(\frac{dV_{oc}}{dt}\right)^{-1} \quad (2)$$

where k is the Boltzmann constant, T is the absolute temperature, and q is the positive elementary charge. The electron lifetime as a function of V_{oc} is shown in Fig. 5b and two features can be found. First, the electron lifetime increases with decreasing V_{oc} (corresponding to the decrease of the decay rate dV_{oc}/dt as shown in Fig. 5a). This is because that the driving force for the electron-hole recombination comes from the V_{oc}, which equals to the difference of the quasi-Fermi levels between n-ZnO and p-CdTe. Second, the electron lifetime for the ZnO/TiO_2/CdTe NRASCs becomes remarkably longer as the TiO_2 layer increasing from 0 to 2 nm. In particular, when the V_{oc} is near 0.1 V , the electron lifetime for the ZnO/TiO_2 (2 nm)/CdTe NRASC becomes three orders of magnitude longer than that for the ZnO/CdTe NRASC. This result, consistent with the J-V characteristics and the impedance spectra, again indicates that the TiO_2 here acts exactly as the passivation and blocking layer and can efficiently suppress the charge recombination at the interface.

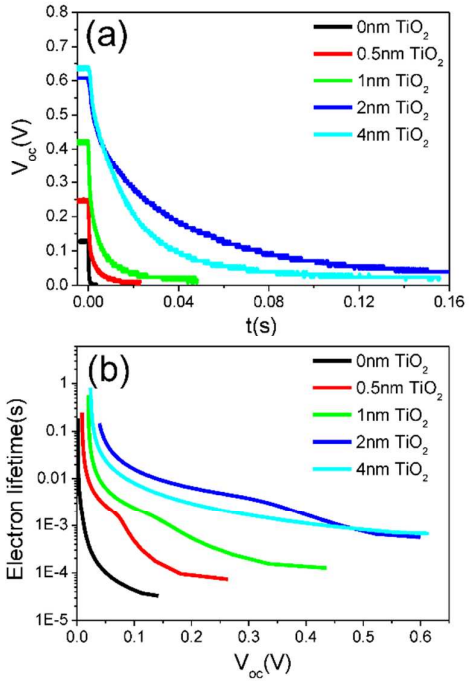

Fig. 5 Open-circuit voltage decay measurement for the ZnO/TiO_2/CdTe NRASCs at room temperature. (a) V_{oc}–time decay curves. (b) Electron lifetime as a function of V_{oc}.

Conclusions

In summary, all-inorganic solid-state ZnO/CdTe NRASCs have been successfully fabricated by depositing p-type CdTe shell onto the ZnO NRs with a simple low-temperature and low-cost solution-based SILAR method. To improve the performance of the ZnO/CdTe NRASC and reduce the charge recombination at the interface, a thin uniform TiO_2 layer was introduced at the ZnO/CdTe interface using ALD technique. The effect of TiO_2 layer on the performances of the solar cells has been systematically investigated. We find that the open-circuit voltage dramatically increases from 165 mV for the ZnO/CdTe NRASC to 627 mV for the ZnO/TiO_2 (4 nm)/CdTe NRASC while the corresponding short-circuit current density and fill factor also improve slightly. The overall power conversion efficiency of the ZnO/TiO_2 (4 nm)/CdTe NRASC can be improved dramatically and reach up to 1.44%, which is 6 times of the ZnO/CdTe NRASC. The results of absorbance spectra and transient absorption spectra demonstrate that the TiO_2 interfacial layer has negligible effect on the light absorption and the charge separation efficiency of the solar cells. Through the systematic measurements including photoluminescence, impedance spectroscopy and open-circuit voltage decay, we find that the thin TiO_2 layer can effectively passivate the surface defects of the ZnO NR and act as a blocking layer to efficiently suppress the charge recombination at the interface, resulting in the remarkable increases of the shunt resistance, electron lifetime, V_{oc}, J_{sc}, FF, and therefore the dramatic improvement of the overall power conversion efficiency. Such kind of rational interface engineering can be easily applied to other photovoltaic devices.

Acknowledgements

This work is supported by MOST of China (2011CB921403), NSFC (under Grant Nos. 11374274, 11074231, 11474260 and 21421063) as well as by the Strategic Priority Research Program (B) of the CAS (XDB01020000).

Notes and references

1 X. Sheng, D. He, J. Yang, K. Zhu and X. Feng, *Nano Letters*, 2014, **14**, 1848-1852.
2 S. H. Ko, D. Lee, H. W. Kang, K. H. Nam, J. Y. Yeo, S. J. Hong, C. P. Grigoropoulos and H. J. Sung, *Nano Letters*, 2011, **11**, 666-671.
3 E. C. Garnett, M. L. Brongersma, Y. Cui and M. D. McGehee, in *Annual Review of Materials Research, Vol 41*, eds. D. R. Clarke and P. Fratzl, 2011, vol. 41, pp. 269-295.
4 J. Zhu, C.-M. Hsu, Z. Yu, S. Fan and Y. Cui, *Nano Letters*, 2010, **10**, 1979-1984.
5 E. Garnett and P. Yang, *Nano Letters*, 2010, **10**, 1082-1087.
6 M. D. Kelzenberg, S. W. Boettcher, J. A. Petykiewicz, D. B. Turner-Evans, M. C. Putnam, E. L. Warren, J. M. Spurgeon, R. M. Briggs, N. S. Lewis and H. A. Atwater, *Nat Mater*, 2010, **9**, 239-244.
7 J. Jean, S. Chang, P. R. Brown, J. J. Cheng, P. H. Rekemeyer, M. G. Bawendi, S. Gradecak and V. Bulovic, *Advanced Materials*, 2013, **25**, 2790-2796.
8 Q. Cui, C. Liu, F. Wu, W. Yue, Z. Qiu, H. Zhang, F. Gao, W. Shen and M. Wang, *Journal of Physical Chemistry C*, 2013, **117**, 5626-5637.
9 M. J. Jin, X. Y. Chen, Z. M. Gao, T. Ling and X. W. Du, *Nanotechnology*, 2012, **23,** 485401.
10 D.-Y. Son, J.-H. Im, H.-S. Kim and N.-G. Park, *Journal of Physical Chemistry C*, 2014, **118**, 16567-16573.
11 J. Xu, Z. H. Chen, J. A. Zapien, C. S. Lee and W. J. Zhang, *Advanced Materials*, 2014, **26**, 5337-5367.

12 X. N. Wang, H. J. Zhu, Y. M. Xu, H. Wang, Y. Tao, S. Hark, X. D. Xiao and Q. A. Li, *Acs Nano*, 2010, **4**, 3302-3308.
13 W. Hao, W. Tian, W. Xina, L. Rong, W. Baoyuan, W. Hanbin, X. Yang, Z. Jun and D. Jinxia, *Journal of Materials Chemistry*, 2012, **22**, 12532-12537.
14 J. Briscoe, D. E. Gallardo, S. Hatch, V. Lesnyak, N. Gaponik and S. Dunn, *Journal of Materials Chemistry*, 2011, **21**, 2517-2523.
15 G. Zhang, S. Jiang, Y. Lin, W. Ren, H. Cai, Y. Wu, Q. Zhang, N. Pan, Y. Luo and X. Wang, *Journal of Materials Chemistry A*, 2014, **2**, 5675-5681.
16 J.-J. Wang, T. Ling, S.-Z. Qiao and X.-W. Du, *Acs Applied Materials & Interfaces*, 2014, **6**, 14718-14723.
17 L. Alibabaei, B. H. Farnum, B. Kalanyan, M. K. Brennaman, M. D. Losego, G. N. Parsons and T. J. Meyer, *Nano Letters*, 2014, **14**, 3255-3261.
18 J. J. Tian, Q. F. Zhang, L. L. Zhang, R. Gao, L. F. Shen, S. G. Zhang, X. H. Qu and G. Z. Cao, *Nanoscale*, 2013, **5**, 936-943.
19 X. T. Yin, W. X. Que, D. Fei, H. X. Xie and Z. L. He, *Electrochimica Acta*, 2013, **99**, 204-210.
20 K. E. Roelofs, T. P. Brennan, J. C. Dominguez, C. D. Bailie, G. Y. Margulis, E. T. Hoke, M. D. McGehee and S. F. Bent, *Journal of Physical Chemistry C*, 2013, **117**, 5584-5592.
21 A. K. Chandiran, M. K. Nazeeruddin and M. Gratzel, *Advanced Functional Materials*, 2014, **24**, 1615-1623.
22 H. Lee, M. K. Wang, P. Chen, D. R. Gamelin, S. M. Zakeeruddin, M. Gratzel and M. K. Nazeeruddin, *Nano Letters*, 2009, **9**, 4221-4227.
23 Y. Tak, S. J. Hong, J. S. Lee and K. Yong, *Journal of Materials Chemistry*, 2009, **19**, 5945-5951.
24 J. Xu, C.-Y. Luan, Y.-B. Tang, X. Chen, J. A. Zapien, W.-J. Zhang, H.-L. Kwong, X.-M. Meng, S.-T. Lee and C.-S. Lee, *Acs Nano*, 2010, **4**, 6064-6070.
25 L. E. Greene, M. Law, D. H. Tan, M. Montano, J. Goldberger, G. Somorjai and P. D. Yang, *Nano Letters*, 2005, **5**, 1231-1236.
26 L. E. Greene, B. D. Yuhas, M. Law, D. Zitoun and P. Yang, *Inorganic Chemistry*, 2006, **45**, 7535-7543.
27 J. Jasieniak, B. I. MacDonald, S. E. Watkins and P. Mulvaney, *Nano Letters*, 2011, **11**, 2856-2864.
28 X. Z. Wu, *Solar Energy*, 2004, **77**, 803-814.
29 R. W. Miles, G. Zoppi and I. Forbes, *Materials Today*, 2007, **10**, 20-27.
30 P. Ravirajan, A. M. Peiro, M. K. Nazeeruddin, M. Graetzel, D. D. C. Bradley, J. R. Durrant and J. Nelson, *Journal of Physical Chemistry B*, 2006, **110**, 7635-7639.
31 H. Ohkita, S. Cook, Y. Astuti, W. Duffy, S. Tierney, W. Zhang, M. Heeney, I. McCulloch, J. Nelson, D. D. C. Bradley and J. R. Durrant, *Journal of the American Chemical Society*, 2008, **130**, 3030-3042.
32 K.-C. Wang, J.-Y. Jeng, P.-S. Shen, Y.-C. Chang, E. W.-G. Diau, C.-H. Tsai, T.-Y. Chao, H.-C. Hsu, P.-Y. Lin, P. Chen, T.-F. Guo and T.-C. Wen, *Sci Rep-Uk*, 2014, **4,** 4756.
33 M. Graetzel, R. A. J. Janssen, D. B. Mitzi and E. H. Sargent, *Nature*, 2012, **488**, 304-312.
34 I. Mora-Sero, S. Gimenez, F. Fabregat-Santiago, R. Gomez, Q. Shen, T. Toyoda and J. Bisquert, *Accounts of Chemical Research*, 2009, **42**, 1848-1857.
35 H. Xue, N. Pan, R. Zeng, M. Li, X. Sun, Z. Ding, X. Wang and J. G. Hou, *Journal of Physical Chemistry C*, 2009, **113**, 12715-12718.
36 E. G. Barbagiovanni, V. Strano, G. Franzo, I. Crupi and S. Mirabella, *Applied Physics Letters*, 2015, **106**, 093108 (093104 pp.)-093108 (093104 pp.).
37 F. Fabregat-Santiago, G. Garcia-Belmonte, I. Mora-Sero and J. Bisquert, *Physical Chemistry Chemical Physics*, 2011, **13**, 9083-9118.
38 Q. Wang, J. E. Moser and M. Gratzel, *Journal of Physical Chemistry B*, 2005, **109**, 14945-14953.
39 J. J. Tian, Q. F. Zhang, E. Uchaker, R. Gao, X. H. Qu, S. E. Zhang and G. Z. Cao, *Energy & Environmental Science*, 2013, **6**, 3542-3547.
40 J. J. Tian, Q. F. Zhang, E. Uchaker, Z. Q. Liang, R. Gao, X. H. Qu, S. G. Zhang and G. Z. Cao, *Journal of Materials Chemistry A*, 2013, **1**, 6770-6775.
41 A. Zaban, M. Greenshtein and J. Bisquert, *Chemphyschem*, 2003, **4**, 859-864.
42 J. Kim, H. Choi, C. Nahm, J. Moon, C. Kim, S. Nam, D. R. Jung and B. Park, *Journal of Power Sources*, 2011, **196**, 10526-10531.
43 J. Bisquert, A. Zaban, M. Greenshtein and I. Mora-Sero, *Journal of the American Chemical Society*, 2004, **126**, 13550-13559.